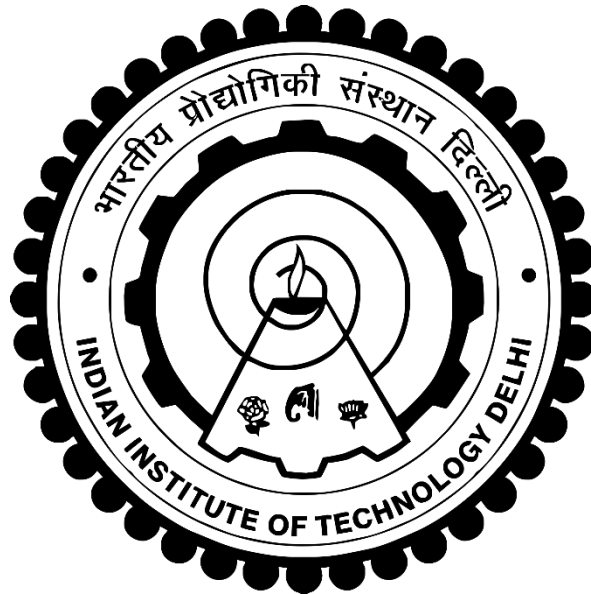


**DESIGN, FABRICATION, AND
CHARACTERIZATION OF LIQUID CRYSTAL
INFILTRATED ELECTRO-OPTIC DEVICES
AND FIBER OPTIC SENSORS**

RAHUL



**DEPARTMENT OF PHYSICS
INDIAN INSTITUTE OF TECHNOLOGY DELHI
NOVEMBER 2024**

© Indian Institute of Technology Delhi (IITD), New Delhi, 2024

**DESIGN, FABRICATION, AND
CHARACTERIZATION OF LIQUID CRYSTAL
INFILTRATED ELECTRO-OPTIC DEVICES
AND FIBER OPTIC SENSORS**

by

RAHUL

Department of Physics

Submitted

in fulfillment of the requirements of the degree of Doctor of Philosophy

to the



INDIAN INSTITUTE OF TECHNOLOGY DELHI

NOVEMBER 2024

Dedicated to my Parents and Supervisor

CERTIFICATE

This is to certify that the thesis entitled, "**Design, fabrication, and characterization of liquid crystal infiltrated electro-optic devices and fiber optic sensors**", being submitted by **Mr. Rahul** to the Indian Institute of Technology Delhi for the award of the degree of **Doctor of Philosophy** in Physics is a record of bonafide research work carried out by him. He has worked under my supervision and guidance and has fulfilled the requirements for the submission of this thesis, which to the best of my knowledge has reached the requisite standard.

The contents of this thesis have not been submitted in part or in full to any other university or institute for the award of any degree or diploma.

Prof. Aloka Sinha

Department of Physics Indian Institute of Technology Delhi

Hauz Khas, New Delhi-110016, India

ACKNOWLEDGEMENTS

I would like to express my deepest gratitude to everyone who has taken part directly and indirectly in my research journey and helped me to shape the thesis. This research work could become possible with the contribution of numerous individuals who gave me their time, expertise, and support in various forms, ranging from insightful discussions and feedback to technical assistance and encouragement. I am profoundly grateful for their invaluable contributions.

First and foremost, I am incredibly indebted to my supervisor, Prof. Aloka Sinha, who provided me the opportunity to work on the fascinating research domain of optics of liquid crystals. Her continuous support, encouragement, and motivation have been instrumental in completing this thesis. She always motivated me to explore new research ideas and achieve the highest milestone. She introduced me to the incredible experience of immersing myself in experimental environments, allowing me to truly understand the essence of making things independently. She always encouraged and helped me shape myself for new startup companies and develop high skill sets. Throughout the years, she has provided me with moral values, career advice, and social and scientific ethics, which helped me in growing as a good human being. Her expertise and encouragement have been instrumental in shaping this work. I am thankful for her invaluable guidance, unwavering support, and constructive feedback throughout the entire process of this thesis. My appreciation for her cannot be enough; I would like to thank you, Madam, for being there and believing in my abilities.

I am also indebted to my research committee members, Prof. R. K. Varshney (Department of Physics, IIT Delhi), Prof. M. R. Shenoy (Department of Physics, IIT Delhi), and Prof. Abhishek Dixit (Department of Electrical Engineering, IIT Delhi), who devoted their precious time during research progress meetings. I am thankful to them for providing valuable insights, suggestions, and constant encouragement regarding research work during the entire period, which have significantly enriched the quality of this research.

I would like to acknowledge the central research facility (CRF), the nanoscale research facility (NRF), and the Physics Department IIT Delhi for providing me with the research facilities. DRDO, CSIR-HRDG India and IIT Delhi are gratefully acknowledged for providing PhD research fellowship during this tenure. I express my sincere thanks to the faculty and the staff members of the Physics Department at IIT Delhi for their cooperative and supportive attitude and for being of great help.

Special thanks go to my senior colleague, Dr. Mukesh Kumar Sharma, for his invaluable guidance and mentorship in the initial months of my PhD. More than just imparting technical knowledge, he has also instilled in me important moral values that I will carry with me throughout my career and life. His integrity, compassion, and dedication serve as constant inspirations for me.

I would like to extend my sincerest appreciation to all the lab members whose contributions have been invaluable to my collective progress and success. I wish to thank Dr. Amina Nafees, Dr. Susanta Chakraborty, Dr. Sourav Patranabish, Dr. Asha Kumari, Ms. Aysha Rani, Ms. Shilpi Bose, Mr. Vaibhav Sharma, Mr. Rishikesh Kushawaha, Mr. Deepak Verma, Mr. Dhananjay Mandal, Mr. Harish Khan, Mr. Kaustav Jit Bora, Mr. Debashish Bag, Ms. Akriti, Mr. Aman and Mr. Deepak Kararwal. Beyond the laboratory, I am grateful for the friendship that we have shared. The laughter, shared experiences, and mutual support have not only enhanced the professional growth but have also created lasting bonds that I will always appreciate.

My respected parents deserve special recognition, without which the acknowledgments would be incomplete. I extend my heartfelt appreciation to my parents Mr. Hare Kishan and Mrs. Pista devi, whose sacrifices have been the guiding forces behind my academic journey. Their unconditional support and sacrifice have helped me reach where I am today. Their endless encouragement during moments of doubt and their celebration of my achievements have propelled me forward. I am deeply grateful to my grandfather, Mr. Jagdish Chand, my brother, Mr. Lalit Kumar, and his wife, who believed in my strength and abilities and always dreamt of my success. To my beloved wife, Mrs. Kirti, your unwavering support, understanding, and patience have been my source of strength throughout this endeavor. During academic pursuits, I have realized the purest form of inspiration, my daughter, Ms. Shanvi, whose innocent laughter and boundless energy have constantly motivated me. I am thankful to all my family members and in-laws members for their support, understanding, and encouragement, which have sustained me through the challenges of this academic journey.

November 2024
New Delhi.

Rahul

ABSTRACT

The electrically tunable electro-optic component and photonics devices are the potential bridge in the advancement of next-generation integrated optical devices, photonics circuits, and display systems. Liquid crystals (LC) are the emerging material for developing electro-optics and optoelectronic devices due to their intriguing properties, such as low driving power, high electro-optic coefficient, and transparency in the visible and infrared spectrum. The use of LC with polymers in the development of electro-optic devices makes them efficient, cost-effective, and biocompatible components, which can be further explored as flexible devices. The LC can be used as a core or cladding medium of compact optical waveguides, a propagation medium in beam steering devices, and an electrically controlled microlens array.

The liquid crystal cladding-based optical waveguides comprise a polymer core that propagates the light through it. The optical properties of LC cladding are tunable, which alters the propagation characteristics of transverse electric (TE) and transverse magnetic (TM) polarized light in the core. The LC waveguide-based optical attenuators and electro-optic switches can be realized using such geometries. In the LC core waveguide, the LC acts as the waveguiding medium sandwiched between the polymer cladding layers. The propagation direction of the guided beam can be changed by developing appropriate electrode patterns on the substrates. The triangular shape pattern of electrodes results in the LC core's electro-optic prism, which causes the polarization-dependent electrically controlled beam steering in the planar waveguides. In the LC waveguides, the fringing field plays a significant role in limiting the steering angles; therefore, the exclusive utilization of the fringing field results in a gradient refractive index that can be used for large-angle beam steering devices. The steering of the light beam towards a common point using the LC medium integrated with a polymer layer is accomplished as electrically tunable lenses.

The aim of the thesis is to explore the effective utilization of the nematic LC with polymers in the development of compact, efficient, cost-effective electro-optics devices for guided wave optics, integrated circuit components, and three-dimensional display systems. The work focuses on developing integrated waveguides using polymers and LC films to present optical attenuators, beam steering devices, and further advanced beam steering devices using fringing fields in LC. The integration of the LC with polymer concave microlenses on the flexible polymer substrates makes them varifocal and flexible microlens arrays. Towards the end of the thesis, the integration of free-standing polymer film with guided wave optics is investigated to demonstrate an acoustic sensor, and the potential application of LC in the fiber cantilever systems in various fields is discussed.

In the first and second chapters of the thesis, the introduction and classification of the LC, the background of optical waveguides, and their fabrication as well as characterization methods are discussed. In the third chapter, we fabricated a planar optical waveguide using negative photoresist AZ15nXT as the waveguiding medium and LC as the upper cladding, demonstrated as a low-threshold optical attenuator. The waveguide operates at a low voltage of 1-4 volts and attenuates TM modes when voltage is applied with a maximum extinction ratio of 12 dB. Then, we used the LC layer in the core of the waveguide, and a polymer Polyvinyl alcohol (PVA) is used as the cladding of the waveguide, which is discussed in chapter 4. A pattern of triangular electrodes is developed on one substrate such that the tunable refractive index prisms induce in the LC core when voltage is applied across the waveguide. The LC prisms steer the propagated beam in the plane of the planar waveguide. In the presence of an electric field across the LC core, the TE and TM polarized light steering in opposite directions. A maximum steering angle of 7.3° is achieved for TM polarization at an applied voltage of $13 V_{pp}$. Then, we investigated beam steering using the effect of fringing fields in LC.

In the fifth chapter, a non-mechanical multidirectional beam steering device is fabricated using a pattern of an electrode system, which comprises a square aperture of the electrode-free

zone. The light beam passes through the aperture of the LC cell, interacts with the fringing field of LC, and steers in the direction of the gradient refractive index. A maximum steering angle of 12° is achieved in this configuration, and the tunability of the direction of the light beam is demonstrated on a two-dimensional plane by applying the voltage to different electrodes. The concept of beam steering can be adequately employed to realize the lenses where all the light beams steer towards a common point recognized as a focal point.

In chapter 6, we developed a concave microlens array using photocurable polymer NOA65 on the Polyethylene terephthalate (PET) substrate. The nematic LC is filled in the cavities of the concave lens and realized flexible LC microlens arrays with electrically tunable focal lengths. The flexibility and tunability of the microlens arrays make them promising components to be used in near-eye virtual reality technology and three-dimensional displays through integral imaging. The polymer films play a significant role in the electro-optics as well as acousto-optics systems. The possibilities for efficient utilization of polymer films in acoustic sensors are also explored. In chapter 7, we have extended this work by integrating a free-standing polymer film on the tip of an optical fiber cantilever and established a highly sensitive acoustic sensor. As a first step, we developed a polyvinylidene fluoride (PVDF) film on the fiber cantilever, which oscillates according to the frequency of sound waves. The dynamic range of the sensor is demonstrated as 100 Hz to 4000 Hz, and a high signal-to-noise ratio of 70 dB is achieved. Towards the end of this chapter, we discussed the feasibility of the extension of this work by developing the LC-embedded polymers and elastomers on fiber cantilevers, which can be potentially recognized in biosensing and soft robotics applications. The electro-optic devices reported in the thesis can be explored by using other polymers and fast-switching LCs that can create new avenues for the development of contemporary photonics.

सारांश

विद्युत रूप से ट्यून करने योग्य इलेक्ट्रो-ऑप्टिक घटक और फोटोनिक्स डिवाइस अगली पीढ़ी के एकीकृत ऑप्टिकल उपकरणों, फोटोनिक्स सर्किट और डिस्प्ले सिस्टम की उन्नति में संभावित पुल हैं। लिक्विड क्रिस्टल (LC) इलेक्ट्रो-ऑप्टिक्स और ऑप्टोइलेक्ट्रॉनिक उपकरणों को विकसित करने के लिए उभरती हुई सामग्री हैं, जैसे कि कम ड्राइविंग पावर, उच्च इलेक्ट्रो-ऑप्टिक गुणांक, और दृश्यमान और अवरक्त स्पेक्ट्रम में पारदर्शिता। इलेक्ट्रो-ऑप्टिक उपकरणों के विकास में पॉलिमर के साथ LC का उपयोग उन्हें कुशल, लागत प्रभावी और जैव-संगत घटक बनाता है, जिसे आगे लचीले उपकरणों के रूप में खोजा जा सकता है। LC का उपयोग कॉम्पैक्ट ऑप्टिकल वेवगाइड के कोर या क्लैडिंग माध्यम, बीम स्टीयरिंग उपकरणों में एक प्रसार माध्यम और एक विद्युत नियंत्रित माइक्रोलेंस सरणी के रूप में किया जा सकता है।

लिक्विड क्रिस्टल क्लैडिंग-आधारित ऑप्टिकल वेवगाइड में एक बहुलक कोर होता है जो इसके माध्यम से प्रकाश का प्रचार करता है। LC क्लैडिंग के ऑप्टिकल गुण ट्यूनेबल हैं, जो कोर में अनुप्रस्थ इलेक्ट्रिक (TE) और अनुप्रस्थ चुंबकीय (TM) ध्रुवीकृत प्रकाश की प्रसार विशेषताओं को बदल देता है। LC वेवगाइड-आधारित ऑप्टिकल एटेन्यूएटर और इलेक्ट्रो-ऑप्टिक स्विच को ऐसी ज्यामिति का उपयोग करके महसूस किया जा सकता है। LC कोर वेवगाइड में, LC बहुलक क्लैडिंग परतों के बीच सैंडविच किए गए वेवगाइडिंग माध्यम के रूप में कार्य करता है। सबस्ट्रेट पर उपयुक्त इलेक्ट्रोड पैटर्न विकसित करके निर्देशित बीम की प्रसार दिशा को बदला जा सकता है। इलेक्ट्रोड के त्रिकोणीय आकार पैटर्न के परिणामस्वरूप LC कोर के इलेक्ट्रो-ऑप्टिक प्रिज्म होते हैं, जो प्लानर वेवगाइड में ध्रुवीकरण-निर्भर विद्युत नियंत्रित बीम स्टीयरिंग का कारण बनता है। LC वेवगाइड्स में, फ्रिजिंग क्षेत्र एक महत्वपूर्ण भूमिका निभाता है, जो स्टीयरिंग कोणों को सीमित करता है; इसलिए, फ्रिजिंग क्षेत्र के अनन्य उपयोग के परिणामस्वरूप एक ढाल अपवर्तक सूचकांक होता है जिसका उपयोग बड़े-कोण बीम स्टीयरिंग उपकरणों के लिए किया जा सकता है। LC माध्यम का उपयोग करके एक सामान्य बिंदु की ओर प्रकाश किरण का स्टीयरिंग एक बहुलक परत के साथ एकीकृत होता है जो विद्युत रूप से ट्यून करने योग्य लेंस के रूप में पूरा होता है।

थीसिस का उद्देश्य निर्देशित तरंग प्रकाशिकी, एकीकृत सर्किट घटकों और तीन आयामी प्रदर्शन प्रणालियों के लिए कॉम्पैक्ट, कुशल, लागत प्रभावी इलेक्ट्रो-ऑप्टिक्स उपकरणों के विकास में पॉलिमर के साथ नेमेटिक LC के प्रभावी उपयोग का पता लगाना है। यह काम LC में फ्रिजिंग क्षेत्रों का उपयोग करके ऑप्टिकल एटेन्यूएटर्स, बीम स्टीयरिंग डिवाइस और आगे उन्नत बीम स्टीयरिंग डिवाइस पेश करने के लिए पॉलिमर और LC फिल्मों का उपयोग करके एकीकृत वेवगाइड विकसित करने पर केंद्रित है। लचीले बहुलक सबस्ट्रेट पर बहुलक अवतल माइक्रोलेंस के साथ LC का एकीकरण उन्हें वैरिफोकल और लचीले माइक्रोलेंस सरणियों बनाता है। थीसिस के अंत में, निर्देशित तरंग प्रकाशिकी के साथ मुक्त खड़े बहुलक फिल्म के एकीकरण की जांच एक ध्वनिक सेंसर को प्रदर्शित करने के लिए की जाती है और विभिन्न क्षेत्रों में फाइबर ब्रैकट सिस्टम में LC के संभावित अनुप्रयोग पर चर्चा की जाती है।

थीसिस के पहले और दूसरे अध्यायों में, LC का परिचय और वर्गीकरण, ऑप्टिकल वेवगाइड की पृष्ठभूमि, और उनके निर्माण के साथ-साथ लक्षण वर्णन विधियों पर चर्चा की जाती है। तीसरे अध्याय में, हमने नकारात्मक फोटोरेसिस्ट AZ15nXT का उपयोग करके एक प्लानर ऑप्टिकल वेवगाइड को वेवगाइडिंग माध्यम और LC को ऊपरी क्लैडिंग के रूप में बनाया, जिसे कम-थ्रेशोल्ड ऑप्टिकल एटेन्यूएटर के रूप में प्रदर्शित किया गया। वेवगाइड 1-4 वोल्ट के कम वोल्टेज पर काम करता है और TM मोड को क्षीण करता है जब वोल्टेज को 12 dB के अधिकतम विलुप्त होने के अनुपात के साथ लागू किया जाता है। फिर, हमने वेवगाइड के मूल में LC परत का उपयोग किया, और एक बहुलक पॉलीविनाइल अल्कोहल (PVA) का उपयोग वेवगाइड के क्लैडिंग के रूप में किया जाता है, जिसकी चर्चा अध्याय 4 में की गई है। त्रिकोणीय इलेक्ट्रोड का एक पैटर्न एक सबस्ट्रेट पर विकसित किया जाता है जैसे कि ट्यून करने योग्य अपवर्तक सूचकांक प्रिज्म LC कोर में प्रेरित करते हैं जब वेवगाइड में वोल्टेज लागू होता है। LC प्रिज्म प्लानर वेवगाइड के विमान में प्रचारित बीम को चलाते हैं। LC कोर में एक विद्युत क्षेत्र की उपस्थिति में, TE और TM ने विपरीत दिशाओं में प्रकाश स्टीयरिंग का ध्रुवीकरण किया। 7.3 V_{pp} के लागू वोल्टेज पर TM ध्रुवीकरण के लिए 13° का अधिकतम स्टीयरिंग कोण प्राप्त किया जाता है। फिर, हमने LC में फ्रिजिंग क्षेत्रों के प्रभाव का उपयोग करके बीम स्टीयरिंग की जांच की।

पांचवें अध्याय में, एक गैर-यांत्रिक बहुदिशात्मक बीम स्टीयरिंग डिवाइस एक इलेक्ट्रोड सिस्टम के पैटर्न का उपयोग करके निर्मित किया जाता है, जिसमें इलेक्ट्रोड-मुक्त क्षेत्र का एक वर्ग एपर्चर शामिल होता है। प्रकाश

किरण LC सेल के एपर्चर से गुजरती है, LC के फ्रिंजिंग क्षेत्र के साथ बातचीत करती है, और ढाल अपवर्तक सूचकांक की दिशा में चलती है। इस कॉन्फिगरेशन में 12° का अधिकतम स्टीयरिंग कोण प्राप्त किया जाता है, और प्रकाश किरण की दिशा की ट्यूनबिलिटी को विभिन्न इलेक्ट्रोड पर वोल्टेज लागू करके द्वि-आयामी विमान पर प्रदर्शित किया जाता है। बीम स्टीयरिंग की अवधारणा को लेंस का एहसास करने के लिए पर्याप्त रूप से नियोजित किया जा सकता है जहां सभी प्रकाश बीम एक सामान्य बिंदु की ओर बढ़ते हैं जिसे फोकल पॉइंट के रूप में मान्यता प्राप्त है।

अध्याय 6 में, हमने पॉलीथीन टेरैफ्थैलेट (PET) सबस्ट्रेट पर फोटोक्यूरेबल पॉलिमर NOA65 का उपयोग करके एक अवतल माइक्रोलेंस सरणी विकसित की। नेमेटिक LC अवतल लेंस की गुहाओं में भरा होता है और विद्युत रूप से ट्यून करने योग्य फोकल लंबाई के साथ लचीले LC माइक्रोलेंस सरणियों का एहसास होता है। माइक्रोलेंस सरणियों का लचीलापन और ट्यूनबिलिटी उन्हें अभिन्न इमेजिंग के माध्यम से निकट-आंख आभासी वास्तविकता प्रौद्योगिकी और त्रि-आयामी डिस्प्ले में उपयोग किए जाने वाले आशाजनक घटक बनाती है। बहुलक फिल्मों इलेक्ट्रो-ऑप्टिक्स के साथ-साथ ध्वनि-प्रकाशिकी प्रणालियों में महत्वपूर्ण भूमिका निभाती हैं। ध्वनिक सेंसर में बहुलक फिल्मों के कुशल उपयोग की संभावनाओं का भी पता लगाया जाता है। अध्याय 7 में, हमने एक ऑप्टिकल फाइबर ब्रैकट की नोक पर एक फ्री-स्टैंडिंग पॉलिमर फिल्म को एकीकृत करके इस काम को बढ़ाया है और एक अत्यधिक संवेदनशील ध्वनिक सेंसर स्थापित किया है। पहले कदम के रूप में, हमने फाइबर ब्रैकट पर एक पॉलीविनाइलिडीन फ्लोराइड (PVDF) फिल्म विकसित की, जो ध्वनि तरंगों की आवृत्ति के अनुसार दोलन करती है। सेंसर की गतिशील रेंज को 100 Hz से 4000 Hz के रूप में प्रदर्शित किया गया है, और 70 dB उच्च सिग्नल-टू-शोर अनुपात हासिल किया जाता है। इस अध्याय के अंत में, हमने फाइबर कैंटिलीवर पर LC-एम्बेडेड पॉलिमर और इलास्टोमर्स विकसित करके इस काम के विस्तार की व्यवहार्यता पर चर्चा की, जिसे बायोसेंसिंग और सॉफ्ट रोबोटिक्स अनुप्रयोगों में संभावित रूप से पहचाना जा सकता है। थिसिस में रिपोर्ट किए गए इलेक्ट्रो-ऑप्टिक उपकरणों को अन्य पॉलिमर और फास्ट-स्विचिंग LC का उपयोग करके खोजा जा सकता है जो समकालीन फोटोनिक्स के विकास के लिए नए रास्ते बना सकते हैं।

TABLE OF CONTENTS

CERTIFICATE	i
ACKNOWLEDGEMENTS	ii
ABSTRACT	iv
सारांश	vii
TABLE OF CONTENTS	x
LIST OF FIGURES.....	xiv
LIST OF TABLES.....	xxi
LIST OF SYMBOLS.....	xxii
LIST OF ABBREVIATIONS	xxiii
Chapter 1	1
1.1 Motivation of the thesis	1
1.2 Introduction.....	7
1.2.1 Liquid crystals.....	7
1.2.2 Liquid crystal alignment	10
1.2.3 Electrical properties	10
1.2.4 Optical properties.....	13
1.2.5 Thermal properties	15
1.2.6 Parameters for nematic 5CB	16
1.3 Optical waveguide	17
1.3.1 Planar Waveguide	20
1.4 Applications	27
1.4.1 Optical attenuators	27
1.4.2 Beam steerer.....	28
1.4.3 Microlens arrays.....	30
1.4.4 Fiber optic acoustic sensors	32
1.5 Outline of the thesis:	33

1.6	Chapter-wise description of the thesis:	34
1.7	Conclusion	38
1.8	References.....	38
Chapter 2	44
2.1	Photolithography.....	44
2.1.1	Positive photolithography	45
2.1.2	Negative photolithography.....	47
2.2	Fabrication of LC waveguide and LC cell.....	48
2.3	Characterization methods.....	50
2.3.1	<i>C-V</i> measurement.....	50
2.3.2	LC Texture analysis	52
2.3.3	Optical waveguide characterization	54
2.3.4	Light coupling techniques.....	56
2.3.5	Interferometric method	61
2.4	Error analysis and instrument precision.....	62
2.5	Conclusion	64
2.6	References.....	65
Chapter 3	67
3.1	Introduction.....	67
3.2	Device structure	69
3.3	Simulation.....	70
3.3.1	Modal Analysis	72
3.4	Experiment.....	75
3.4.1	Fabrication	75
3.4.2	Characterization	77
3.5	Results and discussion	79
3.6	Conclusion	83

3.7	References.....	84
Chapter 4.....	86	
4.1	Introduction.....	86
4.2	Device structure	88
4.3	Theoretical analysis	90
4.3.1	Deviation due to refraction	91
4.3.2	Effect of number of prisms	92
4.3.3	Effect of light polarization and voltage on LC prisms.....	93
4.4	Fabrication	97
4.5	Characterization	99
4.6	Results and discussion	100
4.7	Conclusion	104
4.8	References.....	104
Chapter 5.....	107	
5.1	Introduction.....	107
5.2	Device mechanism	108
5.3	Phase Analysis	111
5.4	Results and Discussion	113
5.4.1	One-dimensional beam steering.....	113
5.4.2	Two-dimensional beam steering.....	116
5.5	Conclusion	120
5.6	References.....	121
Chapter 6.....	124	
6.1	Introduction.....	124
6.2	Design of LC-MLA.....	125
6.3	Mathematical analysis.....	126
6.4	Fabrication	130

6.5	Results and discussion	131
6.5.1	Focusing of LC-MLA	132
6.5.2	Imaging through MLA	134
6.5.3	Effect of electric field on LC-MLA	135
6.5.4	Effect of flexibility on viewing angle	138
6.6	Conclusion	140
6.7	References	141
Chapter 7	143
7.1	Introduction	143
7.2	Design and working principle	145
7.3	Simulation	146
7.4	Cantilever fabrication	150
7.5	Experimental setup	151
7.6	Results and discussion	152
7.6.1	Single cantilever system	152
7.6.2	Double cantilever system	156
7.7	Conclusion	160
7.8	References	161
Chapter 8	163
8.1	Conclusion	163
8.2	Future scope	166
LIST OF PUBLICATIONS	169
AUTHOR'S BIOGRAPHY	171

LIST OF FIGURES

Fig. 1.1. Schematic arrangement of molecules in the crystal, liquid crystal, and liquid state.	7
Fig. 1.2. Classification of Liquid crystals depending on the phase and alignment.....	8
Fig. 1.3. Liquid crystal molecule in (a) homogeneous alignment, (b) twisted nematic alignment, (c) homeotropic alignment, (d) Splay deformation, (e) Twist deformation, (f) Bend deformation.....	12
Fig. 1.4. Effect of applied voltage on the reorientation of LC molecules.....	12
Fig. 1.5. The effective refractive index faced by the light for vertical polarization when the LC molecule aligned at an angle (a) θ , (b) $\theta = 0^\circ$, (c) $\theta = 90^\circ$, (d) $\theta = 90^\circ$ for horizontal polarization.....	14
Fig. 1.6. Variation of refractive index of 5CB LC as a function of temperature.....	16
Fig. 1.7. Variation of capacitance of 5CB LC as a function of voltage.....	16
Fig. 1.8. (a) Schematic representation of an optical waveguide, (b) Refractive index profile of the waveguide.....	18
Fig. 1.9. (a) Schematic representation of circular core waveguide (optical fiber), (b) Rectangular channel waveguide, (c) Planar waveguide.....	19
Fig. 1.10. (a) Symmetric planar waveguide, (b) Asymmetric planar waveguide.	20
Fig. 1.11. Variation of normalized propagation constant with V-parameter for symmetric and asymmetric waveguide.....	25
Fig. 1.12. Modal field pattern of the transverse magnetic fundamental, second and third mode.	26
Fig. 1.13. Bending of the light beam due to (a) gradient of thickness and (b) gradient of refractive index.....	29
Fig. 1.14. Convergence of light beam at the focal point due to a plano-convex lens.....	30

Fig. 1.15. (a) Schematic representation of lenticular microlens array (b) spherical microlens array.....	31
Fig. 1.16. Schematic representation of optical fiber cantilever-based acoustic sensor.....	32
Fig. 2.1. Photolithography steps involved in patterning the ITO layer using positive photoresist.	46
Fig. 2.2. Step involved in the patterning using negative photoresist.	48
Fig. 2.3. The steps followed in the fabrication of LC-based optical waveguide.	49
Fig. 2.4. Fitting of C-V curve for finding the constant V_{th} and V_0	51
Fig. 2.5. LC Textures (a) Schlieren texture without preferred alignment, (b) Homogeneous alignment, (c) color change due to reorientation of LC molecule, (d) Homeotropic alignment at high voltages.	53
Fig. 2.6. Experimental setup for the characterization of optical waveguides.	54
Fig. 2.7. Experimental setup for the characterization of LC waveguide.	55
Fig. 2.8. Schematic representation of end-fire coupling of light.	57
Fig. 2.9. Schematic representation of the butt-coupling method.	58
Fig. 2.10. Coupling of light power in the waveguide by prism coupling method.	59
Fig. 2.11. Coupling of light energy in the waveguide by grating coupler.	60
Fig. 2.12. Schematic experimental setup for the polarization interferometry.	61
Fig. 3.1. (a) The cross-sectional and (b) three-dimensional schematic view of the proposed LC cladding polymer waveguide, (c) schematic of TM polarized propagation at 0 volts, (d) $V \gg V_{th}$	69
Fig. 3.2. (a) Variation of capacitance of LC waveguide (b) orientational angle and refractive index of waveguide, with applied voltage.....	71
Fig. 3.3. Variation of normalized propagation constant with V-parameter.	73
Fig. 3.4. Modal field profile of fundamental mode and ninth mode of the waveguide.	73

Fig. 3.5. Penetration of fundamental mode in LC cladding when the refractive of cladding is (a) 1.53, (b) 1.58, and (c) 1.599.	74
Fig. 3.6. (a) Number of propagating modes and refractive index of LC cladding change with applied voltage, (b) variation of the output power of the waveguide as a function of the refractive index of the cladding, (c) variation of output power as a function of applied voltage.	75
Fig. 3.7. Fabrication steps involved in the development of LC cladding waveguide.	76
Fig. 3.8. Schematic of the experimental setup for the characterization of LC cladding waveguide using end-fire coupling.	77
Fig. 3.9. Photograph of the end-fire coupling experimental setup.	78
Fig. 3.10. Schematic of waveguide characterization setup using fiber butt-coupling technique	78
Fig. 3.11. Photograph of butt-coupling of laser beam in the waveguide.	78
Fig. 3.12. (a) The intensity profile of the output beam spot of the waveguide for TM polarization (b) Variation of the output power of TE and TM modes of the waveguide for end-fire coupling.	79
Fig. 3.13. Variation of the output power of TM modes in the waveguide when light is launched using fiber butt-coupling method.	80
Fig. 3.14. Variation of the output power of TM polarized beam with the rotation of analyzer at 0 V _{pp} , 1 V _{pp} , 1.5 V _{pp} , and 4 V _{pp}	81
Fig. 3.15. The experimental and simulated output power of the waveguide with the applied electric field.	82
Fig. 3.16. Switching and relaxation time of the LC cladding waveguide.	83
Fig. 4.1. Schematic diagram of the proposed LC core waveguide-based beam steering device.	88
Fig. 4.2. Variation of capacitance of the LC waveguide with applied voltage.	89

Fig. 4.3. Reorientation of LC molecules when the electric field is applied.....	90
Fig. 4.4. Refraction of light from (a) rarer to denser medium, and (b) denser to rarer medium.	91
Fig. 4.5. Deviation of the laser beam from a single prism (a) when light is incident normally at angle $\theta_{inc} = 0$, (b) when light is incident at some angle $\theta_{inc} \neq 0$	92
Fig. 4.6. (a) Variation of deviation angle with angle of the prism, (b) Schematic of the deviated beam when five prisms are placed in series.	93
Fig. 4.7. Variation of effective refractive index of the LC prism with applied voltage.	94
Fig. 4.8. Deviation of the beam (a) toward the base of the prism for TM polarization (b) towards the apex of the prism for TE polarization. (c) Variation of steering angle with voltage for TE and TM polarization.	95
Fig. 4.9. Fabrication steps used in the development of LC waveguide-based beam steering device.	97
Fig. 4.10. Texture of the LC waveguide observed in POM at an applied voltage of (a) 0 V (b) 5V, (c) 8V, and (d) 10 V.	98
Fig. 4.11. Schematic of the experimental setup for the characterization of the waveguide. ..	99
Fig. 4.12. Steering of the light beam (a) in the absence of EF; (b) at $V=10 V_{pp}$ for TE polarized light; (b) at $V = 10 V_{pp}$ for TM polarized light.	101
Fig. 4.13. Deviation of TM polarized beam at an applied voltage of $0 V_{pp}$, $5 V_{pp}$, $10 V_{pp}$, 15 V_{pp} and $20 V_{pp}$	101
Fig. 4.14. Variation of steering angle with applied voltage.....	101
Fig. 4.15. Switching dynamics of the LC waveguide-based beam steering device.....	103
Fig. 5.1. Schematic of beam steering device utilizes fringing fields.	109
Fig. 5.2. The color fringes in the fringing field region due to the gradient refractive index in a 25 μm thick cell.....	110
Fig. 5.3. Variation of fringing field width with applied voltage.....	111

Fig. 5.4. Schematic of the experimental setup to observe the interference fringes due to GRIN region in EFZ near the electrode edge.	112
Fig. 5.5. Interference fringes in the EFZ due to the fringing fields at (a) 0 V _{pp} , (b) 3 V _{pp} , (c) 5 V _{pp} , (d) 8 V _{pp} , (e) Phase profile of the fringes at different applied voltages, (f) Variation of the slope of phase profile with applied voltage at 60 μm and 70 μm away from the electrode.	113
Fig. 5.6. (a) Schematic of the experimental setup to observe the beam steering and measure steering angle (b) Variation of steering angle with applied voltage when voltage is applied to the left and the right electrode.	114
Fig. 5.7. Deviation of output beam spot when voltage is applied to (a) left electrode, (b) right electrode.	115
Fig. 5.8. Variation of beam steering angle with the divergence of the laser beam.	115
Fig. 5.9. Fabrication process of beam steering device.	116
Fig. 5.10. (a) Schematic design of the two-dimensional beam steering device consisting of a square EFZ surrounded by four electrodes, (b) Schematic of the experimental setup to demonstrate two-dimensional beam steering. (c-j) Linear fringes in the square EFZ when voltage is given to different combination electrodes, the graphs screen shows the corresponding position of the <i>e</i> -beam and <i>o</i> -beam spot on the screen.	118
Fig. 6.1. Liquid crystal active microlens array in the absence of applied voltage, (b) Inactive microlens when voltage is applied.	126
Fig. 6.2. (a) Three-dimensional height profile of the plano-convex lens, (b) Thickness profile of the microlens array.	127
Fig. 6.3. (a) Interference fringes due to the birefringence lens, (b) Interference pattern due to microlens array.	128
Fig. 6.4. Variation of the focal length of the LC-polymer lens with applied voltage.	129

Fig. 6.5. (a) Variation of the refractive index of LC and polymer with wavelength (b) shift of focal length of the lens with wavelength.	129
Fig. 6.6. Fabrication steps involved in the development of LC-polymer-based flexible MLA.	131
Fig. 6.7. Depth profile of the concave microlens.....	132
Fig. 6.8. Experimental setup for the observation of focusing properties of the LC-MLA. ..	133
Fig. 6.9. Photograph of the experimental setup to study the focusing characteristics of LC-MLA.....	133
Fig. 6.10. (a) Pattern of intensity spots observed at the focal plane of MLA, (b) Three-dimensional intensity profile of output light pattern, (c) Line intensity profile of light spots in the horizontal direction, (d) vertical direction.	134
Fig. 6.11. (a) Experimental setup for the observation of focused image formed by the LC-MLA, (b) Focused image of a letter '4' printed on the test chart, (c) Observed the object through LC-MLA, (d) Imaging of the object through LC-MLA.	135
Fig. 6.12. (a) Interference fringes of the LC-MLA, (b) Effect of voltage on the fringes of the lens, (c) Variation of focal length with applied voltage.....	136
Fig. 6.13. Effect of voltage on the focused image formed by the LC-MLA.	137
Fig. 6.14. Viewing angle of the display through LC-MLA in (a) flat state and (b) curved state, (c) bending state of the presented FLC-MLA.	138
Fig. 6.15. (a) Dynamic response of the fabricated FLC MLA at 7 volts, (b) Variation of response time with applied voltage.	140
Fig. 7.1. Schematic representation of the working of acoustic sensor.....	145
Fig. 7.2. Simulation of power coupled from cantilever fiber to output fiber at a deflection of (a) 0 μm , (b) 2 μm and (c) 4 μm with an air gap of 50 μm	146
Fig. 7.3. Variation of transmitted power through the output fiber with the transverse displacement of the cantilevered fiber.	147

Fig. 7.4. Schematic representation of transverse displacement and transverse offset of the cantilever fiber.	148
Fig. 7.5. The sinusoidal deflection of the cantilever beam and the corresponding transmission through output fiber at (a) 0 μm off set, (b) 1.5 μm off set.	149
Fig. 7.6. Variation of output signal amplitude for a given deflection of the cantilever at different offsets.	149
Fig. 7.7. (a) Schematic of the substrate for the drop-casting of PVDF film on the fiber cantilever, (b) Developed PVDF film on the fiber cantilever.	151
Fig. 7.8. (a) Experimental setup for the demonstration of a single cantilever-based microphone (b) Coupling of light from the fiber-pigtailed laser to the fiber-PVDF cantilever.	151
Fig. 7.9. (a) Frequency response of the fiber-PVDF cantilever for different cantilever lengths at 1.5 Pa pressure. (b) Experimental and simulation variation of resonant frequency with the length of the cantilever for fiber and fiber-PVDF cantilever.	153
Fig. 7.10. Variation of maximum signal amplitude with applied pressure at resonant frequencies.	155
Fig. 7.11. Schematic diagram of the experimental setup for the demonstration of double cantilever system.	156
Fig. 7.12. (a) Frequency response of double cantilever system having different size of PVDF film on two fiber cantilevers of length 1 cm, (b) Sensitivities of the fiber-PVDF cantilever and bare fiber cantilever with frequency.	157
Fig. 7.13. Frequency domain FFT spectrum of the sinusoidal signal of frequency 165 Hz.	159

LIST OF TABLES

Table 1.1. The values of the parameters of nematic 5CB LC.....	17
Table 4.1. Materials and Parameters used to fabricate the LC core waveguide	97
Table 7.1. Comparison of the present acoustic sensor with other low-frequency sensors	161

LIST OF SYMBOLS

\hat{n} : Liquid crystal director	ω : Angular frequency
K_{11} : Splay elastic constant	k_0 : Angular wavenumber
K_{22} : Twist elastic constant	λ : Wavelength
K_{33} : Bend elastic constant	n_c : Cladding refractive index
ϵ_0 : Absolute permittivity of free space	n_f : Core-film refractive index
ϵ_{\perp} : Permittivity along short axis of LC	n_s : Substrate refractive index
ϵ_{\parallel} : Permittivity along long axis of LC	ρ : Density
$\Delta\epsilon$: Dielectric anisotropy	Ω : Area of cross-section
C_{\perp} : Capacitance along short axis of LC	T_c : Clearing temperature of LC
C_{\parallel} : Capacitance along long axis of LC	n : Refractive index
E : Electric field vector	β : Propagation constant
H : Magnetic field vector	b : Normalized propagation constant
V_{th} : Threshold voltage	
n_o : Ordinary refractive index	
n_e : Extra-ordinary refractive index	
Δn : Optical anisotropy or Birefringence	

LIST OF ABBREVIATIONS

LC	: Liquid crystal	SMF	: Single-mode fiber
NLC	: Nematic liquid crystal	MO	: Microscope objective
LCW	: Liquid crystal waveguide	IL	: Insertion loss
5CB	: 4-Cyano-4'-pentylbiphenyl	ER	: Extinction ratio
TE	: Transverse electric	EFZ	: Electrode free zone
TM	: Transverse magnetic	MDP	: Minimum detectable pressure
ITO	: Indium tin oxide	SNR	: Signal-to-noise ratio
IPA	: Isopropyl alcohol	POM	: Polarizing optical microscope
PVA	: Polyvinyl alcohol	DSO	: Digital storage oscilloscope
DI	: De-ionized	CCD	: Charged coupled device
RI	: Refractive index	UV	: Ultra violet
dB	: Decibel	TIR	: Total internal reflection
V_{pp}	: Voltage peak-to-peak	GRIN	: Gradient refractive index
MLA	: Microlens array	PET	: Polyethylene terephthalate
FLC-MLA	: Flexible LC microlens array	EF	: Electric field